Surface Grafting of Ru(II) Diazonium-Based Sensitizers on Metal Oxides Enhances Alkaline Stability for Solar Energy Conversion

Rachel Bangle, Renato N. Sampaio, Ludovic Troian-Gautier*, and Gerald J. Meyer*

Department of Chemistry, University of North Carolina at Chapel Hill, Chapel Hill, North Carolina, 27599-3290, United States

Keywords: Diazonium, Electrografting, Metal oxide, Solar water oxidation, Ruthenium polypyridyl, Alkaline stability

Abstract.

The electrografting of $[Ru(ttt)(tpy\text{-}C_6H_4\text{-}N_2^+)]^{3+}$, where "ttt" is 4,4',4''-tri-*tert*-butyl-2,2':6',2''-terpyridine was investigated on several wide band gap metal oxide surfaces (TiO_2, SnO_2, ZrO_2, ZnO, In_2O_3:Sn) and compared to structurally analogous sensitizers that differed only by the anchoring group, i.e. $-PO_3H_2$ and -COOH. An optimized procedure for diazonium electrografting to semiconductor metal oxides is presented that allowed surface coverages that ranged between $4.7x10^{-8}$ and $10.6\ x10^{-8}$ mol cm^{-2} depending on the nature of the metal oxide. FTIR analysis showed the disappearance of the diazonium stretches at 2266 cm^{-1} after electrografting. XPS analysis revealed a characteristic peak of Ru 3d at 285 eV as well as a peak at 531.6 eV that was attributed to O1s in Ti-O-C bonds. Photocurrents were measured to assess electron injection efficiency of these modified surfaces. The electrografted sensitizers exhibited excellent stability across a range of pH spanning from 1 to 14, where classical binding groups such as carboxylic and phosphonic derivatives were hydrolyzed.

Introduction.

Wide band gap metal oxide (MOx) semiconductor materials have applications in batteries, optoelectronics, electrocatalysis, and solar energy conversion.[1–5] Of specific importance to this work, mesoporous nanocrystalline MOx thin films serve as photoanodes or photocathodes for solar energy conversion in dye-sensitized solar cells (DSSC) and dye-sensitized photoelectrosynthesis cells (DSPECs).[4,5] In DSPECs, a photosensitizer, anchored to the photoanode (often TiO_2, SnO_2, or a SnO_2-TiO_2 core-shell material) is excited by sunlight, which causes electron injection into the MOx acceptor states. The oxidized sensitizer is regenerated by electron transfer from a water oxidation catalyst present either in solution or co-adsorbed to the MOx photoanode. This process is repeated several times until the active catalyst is generated, enabling water oxidation to molecular dioxygen and release of protons. These protons then diffuse through a proton exchange membrane to reach the photocathode (usually NiO) where they are converted into molecular dihydrogen.[5,6] Water oxidation with molecular catalysts is most rapid under alkaline conditions in the presence of a buffer base. Unfortunately, these are also conditions that result in significant sensitizer and catalyst desorption with the most common carboxylic acid and phosphonate surface binding groups.[7–11] Thus binding motifs that are stable under alkaline conditions are critically needed for practical application of DSPECs and the realization of solar fuels.

Pioneering work since the 80's has placed ruthenium chromophores at the forefront of MOx sensitizers to visible light. Early reports used mostly ruthenium sensitizers in solution or immobilized in membranes, but the anchoring of said sensitizers to the MOx surface rapidly developed, leading to greater stability and increased charge injection.[12–19] Classical anchoring groups were carboxylic acids and cyanoacrylic derivatives.[9] Several other anchoring groups, including phosphonic acid,[7–10] silatrane,[7–9] hydroxamate,[9,20] acetyl acetonate,[9,21] boronic acid,[9] silane,[9,22,23] and pyridine derivatives[9,24] have been developed since to remediate stability issues or desorption in selected conditions. For instance, carboxylic acids, for which a pKa of around 4.7 is usually accepted, are only stable at pH values smaller than their pKa.[7] This becomes limiting when developing DSPEC devices in aqueous solution for water oxidation. Phosphonic acid derivatives were later introduced to improve aqueous stability and extend the range of pH in which a DSPEC or DSSC can be operated. Indeed, with their higher pKa, sensitizers containing phosphonic acid are more stable in neutral water. Nonetheless, the sensitizers containing phosphonic acid are not

stable at pH greater than 7, a clear mismatch to the alkaline conditions ideal for implementation of water oxidation catalysts.[7]

In this study, we have examined the grafting of diazonium-based ruthenium sensitizers to MOx surfaces (**Scheme 1**) in order to investigate their stability at alkaline pHs. Surface functionalization through diazonium grafting is a widely-used technique for covalent grafting of organic compounds on all forms of carbon, metallic surfaces, and polymers.[25–35] A few recent studies have also shown diazonium grafting to be possible on MOx nanoparticles, but to our knowledge neither the stability nor the functionality of these surfaces have been established.[27,36–40] Here, the electrochemical grafting of a ruthenium terpyridine sensitizer was achieved on mesoporous MOx (TiO_2, SnO_2, ZrO_2, ZnO, indium-doped tin oxide (In_2O_3:Sn)) thin films deposited on fluorine-doped tin oxide (FTO) glass. Structurally analogous ruthenium chromophores bearing carboxylic acid or phosphonic acid groups were used to assess the comparative stability and surface coverage as well as the excited state injection properties. Despite lower injection yields, the diazonium grafted compounds displayed photostability under 100 mW/cm^{-2} illumination in pH 12 aqueous solutions for as long as 24 hours, which greatly outperformed the carboxylic and phosphonate analogues. Furthermore, the pH 12 stability under ambient light was observed for several months. The alkaline stability of diazonium-grafted sensitizers on oxide surfaces presents an opportunity to advance DSPEC applications, while the generality of the process described allows for potential applications to a wide range of technologies that utilize MOx surfaces with molecular components.

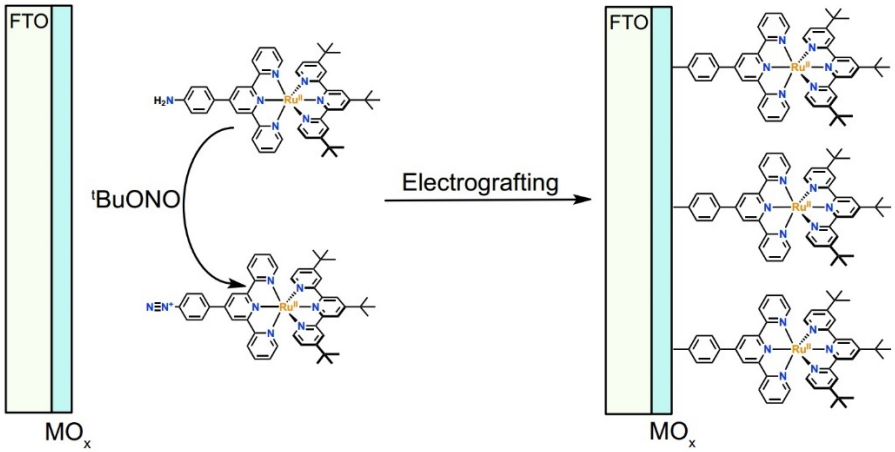

Scheme 1: The general strategy developed for electrografting diazonium-substituted sensitizer molecules on metal oxide (MOx) surfaces. The metal oxides studied here were mesoporous thin

films of metal oxide nanocrystals. The reactive diazonium substituent was generated *in situ* from the reaction between the amine precursor and *tert*-butylnitrite (^{t}BuONO).

Experimental

Materials. The following reagents and substrates were used as received: acetonitrile (CH_3CN, Burdick & Jackson, spectrophotometric grade, 99.9%); deionized water; lithium perchlorate ($LiClO_4$, Aldrich, 99.99%), sodium perchlorate ($NaClO_4$, Aldrich, ≥98.0%); tetra-n-butylammonium perchlorate ($TBAClO_4$, Alfa Aesar, electrochemical grade); titanium(IV) chloride ($TiCl_4$, Aldrich, 99.9%) ; sodium acetate (CH_3COONa, Aldrich, ≥99%); tert-butyl nitrite ($(CH_3)_3CNO_2$, Alfa Aesar, 90%); sodium nitrite ($NaNO_2$, Aldrich, ≥97%); sodium hydroxide (NaOH, Fisher, NF/FCC pellets); perchloric acid ($HClO_4$, Alfa Aesar, 70%); hydrochloric acid (HCl, Fisher, certified ACS Plus); glacial acetic acid (CH_3COOH, Fisher, certified ACS); nitric acid (HNO_3, Fisher, 70%); argon gas (Airgas, >99.998%); poly(ethylene oxide) (Aldrich); poly(ethylene glycol) (Aldrich); terpineol (Aldrich); hydroxypropyl cellulose (HPC, Aldrich); polyethylene glycol copolymer (carbowax, Aldrich); titanium(IV) isopropoxide (Aldrich, 97%); zirconium(IV) isopropoxide (99.9%, Aldrich); zinc oxide nanoparticles (40 wt% in ethanol, <130 nm diameter, Aldrich); tin(IV) dioxide nanoparticles (15 wt% in H_2O, 15 nm diameter, Alfa Aesar); In_2O_3 :Sn nanoparticles (TC8 DE, 20 wt% in ethanol, Evonik Industries) ; fluorine-doped tin oxide-coated glass (FTO, Hartford Glass Co., Inc., 2.3 mm thick, 15Ω/□). Ruthenium trichloride hydrate (Oakwood Chemicals, 97%) and 4,4',4''-tri-*tert*-butyl-2,2':6',2''-terpyridine "ttt" (Sigma-Aldrich) were used as received. NMR solvents were purchased from Cambridge Isotope Laboratories, Inc. Ruthenium 4,4',4''-tri-*tert*-butyl-2,2':6',2''-terpyridine trichloride, [Ru(ttt)Cl_3], tpy-C_6H_4-COOH, tpy-C_6H_4-PO_3Et_2 and tpy-C_6H_4-NH_2 were synthesized according to literature procedures.[41–44]

Synthesis.

[Ru(ttt)(tpy-C_6H_4-COOH)]$^{2+}$.2PF_6^- (Ru-**COOH**).** [Ru(ttt)Cl_3] (52 mg, 0.085 mmol) and tpy-C_6H_4-COOH (31 mg, 0.088 mmol) were place in a microwave tube. Ethanol (10 mL) and N-ethylmorpholine (0.5 mL) were added. The microwave tube was then sealed and heated under microwave irradiation at 120°C for 2 hours. After reaction, 10 mL of water and 2 mL of a saturated NH_4PF_6 aqueous solution were added. The ethanol was removed under reduced pressure and the resulting solid was recovered by filtration and washed with water, small amounts of ethanol, and

diethylether. The product was obtained as a red powder (73 mg, 75%). This compound has been previously reported using a different procedure.[45]

^{1}H NMR (400 MHz, ∂-CD_3CN) δ 9.02 (s, 2H), 8.78 (s, 2H), 8.64 (d, *J* = 8.1 Hz, 2H), 8.51 (d, *J* = 2.1 Hz, 2H), 8.36 (d, *J* = 8.4 Hz, 2H), 8.30 (d, *J* = 8.4 Hz, 2H), 8.04 – 7.86 (m, 2H), 7.36 (d, *J* = 5.5 Hz, 2H), 7.29 – 7.17 (m, 4H), 7.12 (dd, *J* = 6.0, 2.1 Hz, 2H), 1.75 (s, 9H), 1.31 (s, 18H). HRMS (ESI-MS) m/z: $[M-(PF_6)]^+$ Calcd for $C_{49}H_{50}F_6N_6O_2PRu$ 1001.2680; Found 1001.2609.

$[Ru(ttt)(tpy\text{-}C_6H_4\text{-}PO_3Et_2)]^{2+}.2PF_6^-$. (Ru-**$PO_3Et_2$).** $[Ru(ttt)Cl_3]$ (156 mg, 0.256 mmol) and tpy-C_6H_4-PO_3Et_2 (114 mg, 0.256 mmol) were place in a microwave tube. Ethanol (18 mL) and N-ethylmorpholine (1.5 mL) were added. The microwave tube was then sealed and heated under microwave irradiation at 120°C for 2 hours. After reaction, 10 mL of water and 2 mL of a saturated NH_4PF_6 aqueous solution were added. The ethanol was removed under reduced pressure and the resulting solid was recovered by filtration and washed with water, small amounts of ethanol, and diethylether. The product was obtained as a red powder (280 mg, 88%).

^{1}H NMR (400 MHz, ∂-CD_3CN) δ 9.00 (s, 2H), 8.78 (s, 2H), 8.64 (d, *J* = 8.1 Hz, 2H), 8.51 (d, *J* = 2.0 Hz, 2H), 8.36 – 8.27 (m, 2H), 8.12 (dd, *J* = 12.8, 8.3 Hz, 2H), 7.95 (td, *J* = 7.8, 1.5 Hz, 2H), 7.36 (d, *J* = 5.0 Hz, 2H), 7.28 – 7.17 (m, 4H), 7.12 (dd, *J* = 6.0, 2.1 Hz, 2H), 4.19 (ddd, *J* = 8.2, 7.1, 2.8 Hz, 4H), 1.75 (s, 9H), 1.38 (d, *J* = 7.0 Hz, 6H), 1.31 (s, 18H). HRMS (ESI-MS) m/z: : $[M-PF_6]^+$ Calcd for $C_{52}H_{59}F_6N_6O_3P_2Ru$ 1093.3071; Found 1093.3017.

$[Ru(ttt)(tpy\text{-}C_6H_4\text{-}PO_3H_2)]^{2+}.2PF_6^-$ (Ru-**PO_3H_2).** Ru-**PO_3Et_2** (330 mg, 0.266 mmol) was dissolved in 25 mL of CH_3CN. Trimethylsilyl bromide TMSBr (180 µL, 1.34 mmol) was added and the mixture was stirred at 70°C under an argon atmosphere for 24 hours. After reaction, the mixture was brought to room temperature and 5 mL of methanol was added. The resulting solution was stirred for 30 minutes and evaporated to dryness under reduced pressure. The residue was washed with small amounts of cold CH_3CN and diethylether to obtain the title compound as a red powder (297 mg, 94 %).

^{1}H NMR (400 MHz, ∂-CD_3OD) δ 9.31 (s, 2H), 9.08 (s, 2H), 8.90 (d, *J* = 8.1 Hz, 2H), 8.79 (d, *J* = 2.0 Hz, 2H), 8.42 (dd, *J* = 8.0, 3.1 Hz, 2H), 8.16 (dd, *J* = 13.1, 8.0 Hz, 2H), 8.01 (td, *J* = 7.9, 1.5 Hz, 2H), 7.50 – 7.42 (m, 2H), 7.37 (d, *J* = 6.0 Hz, 2H), 7.32 – 7.22 (m, 4H), 1.81 (s, 9H), 1.35 (s, 18H). HRMS (ESI-MS) m/z: : $[M-(PF_6)_2]^{2+}$ Calcd for $C_{48}H_{51}N_6O_3P_1Ru$ 446.1402; Found 446.1389.

$[Ru(ttt)(tpy\text{-}C_6H_4\text{-}NH_2)]^{2+}.2PF_6^-$ (Ru-NH_2). $[Ru(ttt)Cl_3]$ (156 mg, 0.256 mmol) and tpy-C_6H_4-NH_2 (87 mg, 0.268 mmol) were placed in a microwave tube. Ethanol (18 mL) and N-ethylmorpholine (1.5 mL) were added. The microwave tube was then sealed and heated under microwave irradiation at 120°C for 2 hours. If the chloride salt was desired, the solution was evaporated to dryness and the residue was washed with cold ethanol and diethyl ether. If the PF_6^- compound was desired, after reaction, 10 mL of water and 2 mL of a saturated NH_4PF_6 aqueous solution were added. The ethanol was removed under reduced pressure and the resulting solid was recovered by filtration and washed with water, small amounts of ethanol, and diethylether. The product was obtained as a red powder (225 mg, 78%). This compound has been previously reported using a different procedure.[46]

^{1}H NMR (400 MHz, ∂-CD_3CN) δ 8.89 (s, 2H), 8.77 (s, 2H), 8.60 (d, J = 8.2 Hz, 2H), 8.50 (d, J = 2.1 Hz, 2H), 8.00 (d, J = 8.5 Hz, 2H), 7.91 (td, J = 7.9, 1.6 Hz, 2H), 7.31 (d, J = 5.4 Hz, 2H), 7.27 (d, J = 5.9 Hz, 2H), 7.20 – 7.15 (m, 2H), 7.13 (dt, J = 6.0, 3.3 Hz, 2H), 6.95 (d, J = 8.5 Hz, 2H), 4.77 (s, 2H), 1.74 (s, 9H), 1.31 (s, 18H). $[M\text{-}PF_6]^+$ Calcd for $C_{48}H_{51}F_6N_7PRu$ 972.2891; Found 972.2800.

$[Ru(ttt)(tpy\text{-}C_6H_4\text{-}N_2^+)]^{3+}.3PF_6^-$ (Ru-N_2^+). This procedure was inspired by a report in literature.[47] Ru-**NH_2** (75 mg, 0.084 mmol) was dissolved in 12 mL of 0.5 M HCl and brought to 0°C using an ice bath. $NaNO_2$ (15 mg, 0.217 mmol), dissolved in 1 mL of 0.5 M HCl was then added in one portion. The mixture was stirred at 0°C for 3 hours. After reaction, 2 mL of a saturated KPF_6 aqueous solution was added to precipitate the complex. The title compound was isolated as a dark-red powder by filtration and was washed with water, cold ethanol, and diethylether and used without further purification. IR (neat) ν_{max} (cm^{-1}): 3320, 3105, 2960, 2910, 2870, 2266, 1610, 1585, 1475, and 1425.

Nuclear Magnetic Resonance. Characteristic NMR spectra were obtained at room temperature on a Bruker Avance III 400 MHz spectrometer. Solvent residual peaks were used as internal standards for ^{1}H (δ =1.95 ppm for CD_3CN, 3.31 ppm for CD_3OD) and ^{13}C (δ = 77.16 ppm for $CDCl_3$, 39.52 ppm for DMSO) chemical shift referencing. NMR spectra were processed using MNOVA.

Mass Spectrometry. Samples were analyzed with a hybrid LTQ FT (ICR 7T) (ThermoFisher, Bremen, Germany) mass spectrometer. Samples were introduced via a micro-electrospray source at a flow rate of 3 μL/min. Xcalibur (ThermoFisher, Breman, Germany) was

used to analyze the data. Each mass spectrum was averaged over 200 time domains. Electrospray source conditions were set as: spray voltage 4.7 kV, sheath gas (nitrogen) 3 arb, auxiliary gas (nitrogen) 0 arb, sweep gas (nitrogen) 0 arb, capillary temperature 275ºC, capillary voltage 35 V and tube lens voltage 110 V. The mass range was set to 150-2000 m/z. All measurements were recorded at a resolution setting of 100,000. Solutions were analyzed at 0.1 mg/mL or less based on responsiveness to the ESI mechanism. Low-resolution mass spectrometry (linear ion trap) provided independent verification of molecular weight distributions.

UV−Vis Absorption. UV−vis absorption spectra were recorded on a Varian Cary 60 or Cary 50 UV−vis spectrophotometer with a resolution of 1 nm. The molar absorption coefficients were determined by diluting a stock solution of the desired complex and represent averages of at least three independent measurements.

Electrochemistry. Square wave and cyclic voltammetry were performed with a BASi Epsilon potentiostat in a standard three electrode cell in CH_3CN or aqueous electrolytes. The cells consisted of a FTO/MOx electrode and platinum gauze as counter-electrode. A non-aqueous silver/silver chloride electrode (Pine) was used as a reference electrode that was referenced to an internal ferrocene (Fc) standard (630 mV vs. NHE).

Metal Oxide Films. Nanocrystalline anatase TiO_2 (~15 nm diameter) and ZrO_2 (~10 nm diameter) nanoparticles were prepared by acid hydrolysis of Ti(*i*-OPr)$_4$ or Zr(*i*-OPr)$_4$ as described previously.[48] SnO_2 (15 nm diameter) and In_2O_3 :Sn (~15 nm diameter) nanoparticles were prepared from a colloidal SnO_2 suspension, as described previously.[49,50] ZnO nanoparticles (<130 nm diameter) were prepared from a ZnO colloidal suspension by an adjusted previously described procedure.[51] Briefly, 15 g ZnO nanoparticle suspension was stirred and heated to 40˚C while 5% by mass hydroxypropyl cellulose was added. Following overnight stirring, 10 wt% terpineol was added followed by 5 min pulsed horn sonication.

Thin MOx (TiO_2, SnO_2, ZrO_2, ZnO, In_2O_3:Sn) nanoparticle films of approximately 4 μm were prepared by doctor blading onto transparent FTO using ~3.5 μm cellophane tape (3M) as a spacer, followed by sintering for 30 min at 450˚C under oxygen flow and storage at 80˚C. Film thickness and area were determined using a profilometer (Bruker DektatXT Profilometer). Tunneling Electron Microscopy (TEM) was used to capture images of the nanoparticles scraped from the films to measure particle size and gauge film density (See **Figure S1**).

Film Dye Loading. MOx films were dye-loaded with Ru-$\mathbf{PO_3H_2}$ and Ru-**COOH** by immersion for at least 24 hours in a concentrated solution of Ru-$\mathbf{PO_3H_2}$ and Ru-**COOH** in CH_3CN. Films were dye-loaded with Ru-$\mathbf{N_2}^+$ by electrografting with *in situ* generation of Ru-$\mathbf{N_2}^+$ from Ru-$\mathbf{NH_2}$.$2PF_6^-$ by reaction with tert-butyl nitrite. To do so, a 2 mM solution of Ru-$\mathbf{NH_2}$ in 100 mM $TBAClO_4$ CH_3CN electrolyte in a 3 mL cuvette was cooled to 0°C using an ice bath and was sparged with argon for 30 min. After this, *tert*-butyl nitrite (20 µL, 0.15 mmol) was added and the mixture was allowed to react for 10 minutes. An immediate color change from red to purple was noticed. After reaction, a standard three electrode electrochemical setup was introduced, in which the MOx film served as working electrode and a platinum gauze served as counter electrode. Remaining under an argon atmosphere and in an ice bath, TiO_2 films were held at a potential ranging from +100 mV to -100 mV vs. NHE for 30 min. Other metal oxides reached maximal grafting at different applied potentials, as will be discussed (*vide infra)*. Dye-loaded slides were then removed, rinsed with CH_3CN to remove unreacted material and immersed in CH_3CN for at least 30 minutes prior to being used.

Alternatively, an aqueous electrografting method was also developed. A similar procedure was used using Ru-$\mathbf{NH_2}$.$2Cl^-$. The complex was dissolved in 3mL of 0.5 M HCl *(aq)* kept at 0°C and sparged with argon for 30 minutes before reaction with $NaNO_2$ (20 µL 1 M solution, 0.02 mmol). A ~50 mV vs. NHE potential was applied for 30 min. The grafted surface was then washed with water and CH_3CN and soaked in CH_3CN. The aqueous electrografting gave similar absorbance results as the CH_3CN electrografting.

Surface Characterization and Stability. Fourier transform infrared spectroscopy (FTIR) measurements were acquired on both powder and thin film samples using a Bruker model Alpha FTIR spectrophotometer equipped with an Alpha-P attenuated total reflectance (ATR) attachment. 36 spectra with a 2 cm^{-1} resolution were averaged to create the spectra with FTO subtracted as a baseline. X-ray photoelectron spectroscopy (XPS) was performed using a Kratos Axis Ultra-DLD spectrometer (Kratos Analytical Ltd., Manchester, UK) with a base pressure of 5 x 10^{-9} Torr equipped with a monochromatic Al K alpha source and a charge neutralizer. Survey and high-resolution spectra were taken with pass energies of 80 eV and 20 eV, respectively. Binding energies (BE) were found using BE=284.6 eV for C1s as a reference.

Dye-loaded film stability was determined at various pHs in the dark and under illumination. Non-illuminated film stability was determined by soaking the dye-loaded films in water adjusted

at the desired pH. The films were immersed for a specified amount of time and were then rinsed with water adjusted to the same pH prior to UV-vis measurement at the MLCT. Fresh soaking solutions were used for each time point at which significant desorption occurred. When little desorption occurred, slides were analyzed in a single solution. Alternatively, films were placed in water adjusted to the desired pH and constantly illuminated with a 455 nm LED (Thor labs, 100 mW cm^{-2}) while periodic UV-vis measurements at the MLCT were made to determine photostability.

Sensitizer Characterization. Ru(III/II) reduction potentials of the sensitizers were measured on In_2O_3:Sn thin films by spectroelectrochemistry. Spectra were monitored by an Avantes AvaLight DHc light source and an Avantes StarLine AvaSpec-2048 UV/visible spectrophotometer while potentials were applied by a Pine Research Instrumentation (PRI) Wavenow potentiostat controlled by Aftermath software (PRI). In_2O_3:Sn on a FTO thin film served as the working electrode with a platinum gauze counter electrode and Ag/AgCl saturated KCl reference electrode. Dye-loaded thin films were submerged in argon-purged, pH-adjusted aqueous solutions.

Photochemical Analysis. Photocurrents over extended time periods were examined with a home-built H cell using TiO_2 and SnO_2 thin films as working electrodes and platinum gauze as counter electrode. Electrodes were submerged in a nitrogen-saturated aqueous solution of 0.1 M acetate buffer and 0.5 M $NaClO_4$ adjusted to pH 5 or 12. The working and counter electrodes were separated by a Nafion proton-exchange membrane, with 50 mM sacrificial electron donor on the working electrode side (hydroquinone for pH 5 solutions, triethanolamine for pH 12 solutions). An overpotential of 400 mV vs NHE was applied and the cell was illuminated at 1 Sun using a Cole-Parmer Illuminator (41720 series) equipped with a 400 nm filter (Thor labs).

Results

Three ruthenium sensitizers (**Figure 1**) were obtained by reaction of the precursor ruthenium 4,4',4''-tri-*tert*-butyl-2,2':6',2''-terpyridine trichloride, [Ru(ttt)Cl_3] with the corresponding terpyridine ligand in ethanol in the presence of N-ethyl-morpholine. With regard to Ru-$\mathbf{N_2}^+$, it was either isolated by reaction of the parent amino compound (Ru-$\mathbf{NH_2}$) with $NaNO_2$, or generated *in situ* with *tert*-butyl nitrite (^{t}BuONO).

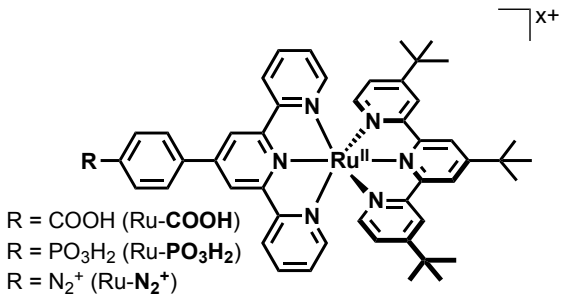

Figure 1: Ruthenium sensitizers used in this study that differ only by their anchoring group (Ru-**COOH,** Ru-**PO_3H_2** or Ru-**N_2^+**). In the case of Ru-**COOH** and Ru-**PO_3H_2**, the overall charge is 2+ whereas in the case of Ru-**N_2^+**, the overall charge is 3+.

These ruthenium sensitizers differed only by their anchoring group, i.e. carboxylic acid (Ru-**COOH**), phosphonic acid (Ru-**PO_3H_2**) or diazonium (Ru-**N_2^+**). The electron donating tri-*tert*-butyl moieties were introduced to the uppermost terpyridine to increase excited state localization on the ligand nearest the surface in order to favor charge injection. The bulkiness of these groups might also prevent polymerization side-reactions that have been previously reported for grafting of diazonium salts.[26,28,36]Meosporous oxide thin films were surface functionalized with Ru-**COOH** or Ru-**PO_3H_2** by overnight reactions in concentrated CH_3CN solutions (dyeing solutions). Functionalization by Ru-**N_2^+** was achieved by an electrografting procedure developed herein and described below.

Electrografting Procedure

The electrografting of Ru-**N_2^+** was first optimized for TiO_2 and was then adjusted for SnO_2, ZnO, ZrO_2, and In_2O_3:Sn. A 2 mM solution of Ru-**NH_2** was reacted with an excess of *tert*-butyl-nitrite in 100 mM $TBAClO_4$ CH_3CN for 10 minutes at 0°C under argon to yield the desired Ru-**N_2^+**. A constant potential ranging from +100 mV to -100 mV vs. NHE was applied for 30 min to the mesoporous nanocrystalline (anatase)TiO_2 thin film. The same procedure achieved grafting on the other MOx slides, but the applied potential that gave the highest surface coverage (termed here "optimal potential") was dependent on the identity of the MOx. Optimal potentials are presented over a 200 mV range for each MOx to account for small variations observed between samples (**Table 1**). The electrografting was nearly insensitive to whether $TBAClO_4$ or $LiClO_4$ electrolyte solutions were used. Both the period of time for which that potential was applied (from 5 to 60 minutes) and the sensitizer concentration (from 0.5 mM to 4 mM) were found to affect the sensitizer surface coverage, but increases in surface coverage were limited beyond the time and sensitizer concentration used herein, *i.e.* 30 minutes and 2 mM.

The sensitizer surface coverage, Γ, was calculated with **Equation 1**, where ε is the

$$\Gamma = \frac{A_{max}}{\varepsilon \times 1000} \qquad (1)$$

sensitizer extinction coefficient (given in Supplementary Information, **Figure S2**), A_{max} is the maximum absorbance value attained on each MOx thin film, and 1000 is a factor to convert from L to cm^3.[52] The Ru-$\mathbf{N_2}^+$ data corresponds to grafting for 30 min from a 2 mM Ru-$\mathbf{N_2}^+$ solution. Surface coverage calculations were complicated by the large spectral shift observed between Ru-$\mathbf{N_2}^+$ in solution and the dyes grafted on the surface (**Figure S2**). This means that the extinction coefficient measured for Ru-$\mathbf{N_2}^+$ gave no information about the surface coverage. To approximate surface coverage in this case, the value 17000 M^{-1} cm^{-1} was used, assuming Ru-$\mathbf{N_2}^+$ on the surface to have a similar extinction coefficient as Ru-$\mathbf{PO_3H_2}$ and Ru-**COOH**, 17500 M^{-1} cm^{-1} and 20900 M^{-1} cm^{-1} respectively. Functionalization with Ru-$\mathbf{PO_3H_2}$ resulted in surface coverages very similar to those measured for Ru-$\mathbf{N_2}^+$ grafting, and functionalization with Ru-**COOH** consistently resulted in lower surface coverages.

Table 1: Surface Coverage and Absorption Maxima of the Dye-Loaded MOx Surfaces

	Ru-$\mathbf{N_2}^+$			Ru-$\mathbf{PO_3H_2}$		Ru-**COOH**	
	Surface Coverage (mol cm^{-2} x 10^{-8})	MLCT Absorption Max (nm)	App. Potential[a] (mV vs NHE)	Surface Coverage (mol cm^{-2} x 10^{-8})	MLCT Absorption Max (nm)	Surface Coverage (mol cm^{-2} x 10^{-8})	MLCT Absorption Max (nm)
TiO_2	8.8	492	100 – -100	10.5	486	2.9	486
SnO_2	5.3	492	225 – 25	3.8	486	1.7	488
ZnO	10.6	491	300 – 100	3.8	485	2.3	486
ZrO_2	4.7	490	-1100 – -1300	4.3	486	2.3	487
In_2O_3:Sn	10.0	491	100 – -100	7.2	485	-[b]	-[b]

[a] The 'optimal' range of applied potentials found to induce maximum surface coverage. [b] Surface functionalization did not occur to an appreciable degree on In_2O_3:Sn.

The amount of grafted sensitizer was found to increase rapidly as more reducing potentials were applied, as seen in **Figure 2**. The "turn on" potential for grafting on TiO_2, SnO_2, and ZnO was significantly more positive than the potential at which reduction of the oxide thin films could be spectroscopically or electrochemically detected (**Figure 2)**. This behavior, however, differed for ZrO_2 and In_2O_3:Sn, for which the grafting was concurrent with current onset. At applied potentials more negative than the "turn on" potential, the surface coverages decreased in what is termed a "turn off." It should be noted that the ZrO_2 grafting did not occur until a potential more negative than the potential "turn off" for the other MOx. Interestingly, no grafting was observed

when TiO_2 films were first reduced electrochemically at -1.0 V (as indicated by color change in the film) and then exposed to Ru-$\mathbf{N_2}^+$; the dark coloration associated with TiO_2 reduction was unchanged with no evidence for surface functionalization. Additionally, when the FTO generally exposed in mesopores was coated and blocked with $TiCl_4$ (described previously) prior to doctor-blading TiO_2, the TiO_2 films grafted Ru-$\mathbf{N_2}^+$ in the same way as films on untreated FTO.[53] Despite these curious phenomena, electrochemical grafting was successfully optimized for TiO_2, SnO_2, ZnO, ZrO_2, and In_2O_3:Sn, **Table 1**.

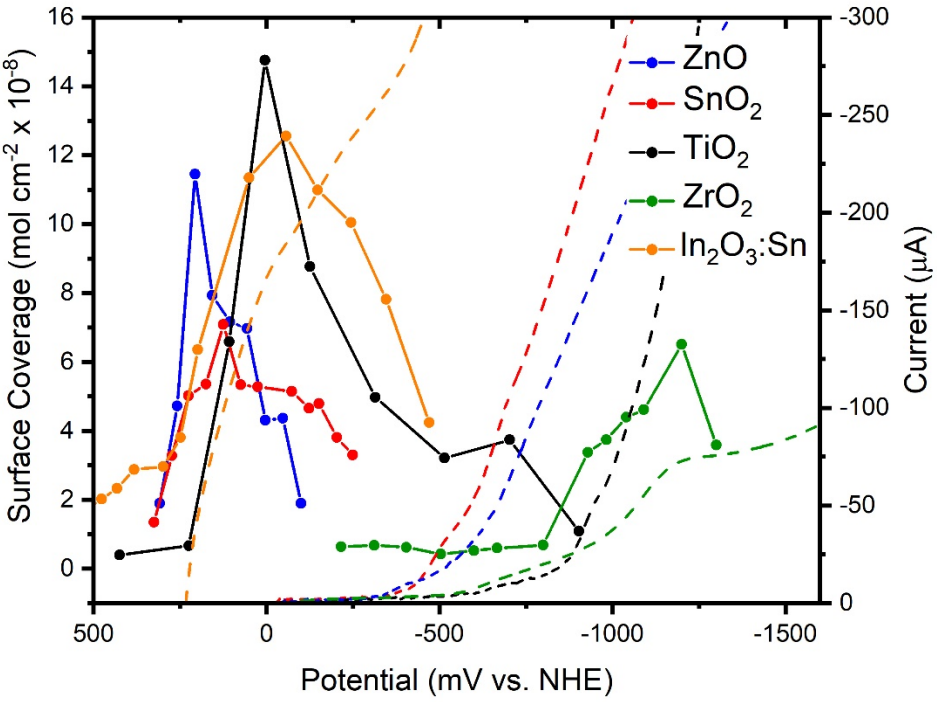

Figure 2: The left hand side shows the surface coverage (solid) as a function of applied potential for TiO_2 (black), SnO_2 (red), ZnO (blue), ZrO_2 (green), and In_2O_3:Sn (orange). Each data point represents a new MOx thin film and the solid lines are present to guide the eye. The surface grafting was performed in 2 mM Ru-$\mathbf{N_2}^+$ in 100 mM $TBAClO_4$ CH_3CN for 30 min. The right-hand side shows linear voltammetry data (dashed) for each undyed MOx film. The voltammetry experiments were performed on undyed films in 100 mM $TBAClO_4$ CH_3CN.

Solution studies were performed to gain insight into chemistry occurring in the dyeing solutions that might account for the inability to graft at more negative applied potentials. In a typical experiment, TiO_2 thin films were submerged in relatively dilute (~0.9 mM) Ar purged, 0˚C Ru-$\mathbf{N_2}^+$ dyeing solutions and held at potentials either more or less reducing than the ideal

electrografting potential for TiO_2 (70 mV and -530 mV vs NHE) for 30 minutes. The electrodes were then removed and the UV-vis spectrum of the remaining Ru-$\mathbf{N_2}^+$ dyeing solution was measured and compared to that of a fresh Ru-$\mathbf{N_2}^+$ solution. The results in **Figure 3** show a significant absorption change after the more negative potential was applied. Similar changes occurred, albeit to a much smaller extent, at open circuit or when a less negative potential was applied. The spectrum measured after reduction bared a marked resemblance to Ru-$\mathbf{NH_2}$ or other ruthenium-bisterpyridine dyes (**Figure 3**).

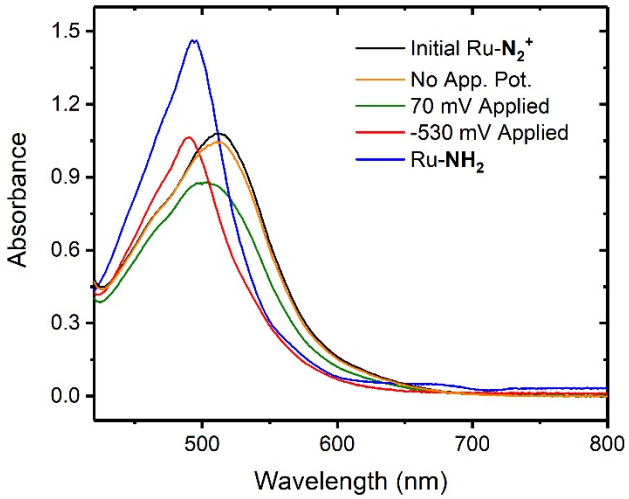

Figure 3: The visible absorption spectra of Ru-$\mathbf{N_2}^+$ dyeing solutions before (black) and after 30 min of standing in solution at 0°C (orange) or applying 70 mV vs NHE (green) or -530 mV vs NHE (red) in comparison to an equal-concentration solution of Ru-$\mathbf{NH_2}$ (blue).

Figure 4 shows the absorbance spectra of the sensitizers in solution and on a representative MOx surface (TiO_2). The absorption was characteristic of metal-to-ligand charge-transfer (MLCT) transitions. The MLCT maximum shifted with the nature of the binding group and was independent of MOx surface, as can be seen in **Table 1** and **Figure S3**. The Ru-$\mathbf{N_2}^+$ grafted thin films had a strongly red-shifted (15 nm) absorbance in CH_3CN solution which was broader and slightly red-shifted (~5 nm) when anchored to the oxide surface as compared to Ru-$\mathbf{PO_3H_2}$ and Ru-**COOH**. It should be noted that though these absorbance values are normalized, maximum attainable surface coverages depended on the nature of the MOx and the binding group. Representative spectra of each sensitizer on each surface are shown in the Supporting Information (**Figure S3**).

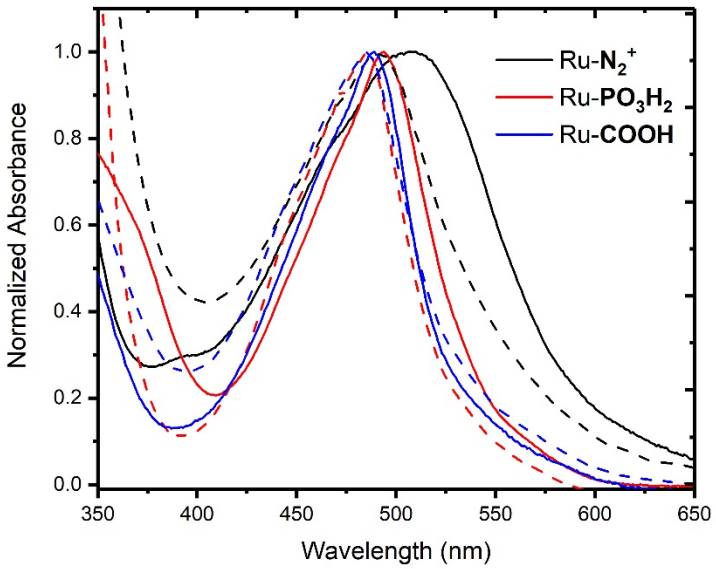

Figure 4: Normalized UV-vis absorbance spectra of Ru-$\mathbf{N_2}^+$ (black), Ru-$\mathbf{PO_3H_2}$ (red), and Ru-**COOH** (blue) in CH_3CN solution (solid) and anchored to TiO_2 (dashed).

Surface Characterization

The nature of the bonds between Ru-$\mathbf{N_2}^+$, Ru-$\mathbf{PO_3H_2}$, and Ru-**COOH** and the surfaces were analyzed by FTIR spectroscopy as solid samples and on all the MOx except In_2O_3:Sn due to its lack of transmittance between 1500 and 4000 cm^{-1}.[54,55] Solid samples of the sensitizers exhibited three characteristic peaks between 2850 and 2970 cm^{-1} corresponding to stretches of the three sensitizer *tert*-butyl groups, a C=C stretching peak at 1610 cm^{-1}, and many shared peaks in the fingerprint region that were independent of the binding group, as indicated in **Figure 5**. Several of these peaks were also present on the dye-loaded MOx surfaces, but were not present in spectra of undyed MOx films, i.e. vibrations at 2960, 2910, 2870, 1610, and 1400 cm^{-1}. These peaks were common to all grafted MOx surfaces. The majority of the peaks are sharp and clear in the solid ruthenium dyes, however, they are significantly broadened and decreased in intensity on the MOx surfaces. Individual peaks are difficult to assign in the 1750-1500 cm^{-1} region for the different metal oxides. However, the broad and sharp absorbance peaks in this region that are metal oxide independent likely correspond to dye absorption. In addition to peaks shared between ruthenium dyes regardless of binding group, sharp peaks were observed in solid Ru-$\mathbf{N_2}^+$ at 2266 and 3320 cm^{-1} that were not present when Ru-$\mathbf{N_2}^+$ was grafted to any MOx surface. Ru-**COOH** dyed MOx films displayed usually sharp C=O stretching peaks at 1730 cm^{-1}, but this peak was notably broader on TiO_2. Additionally, a peak at 1544 cm^{-1} was present on all MOx surfaces grafted with Ru-$\mathbf{N_2}^+$ that did not appear in the solid sample or on surfaces functionalized with Ru-$\mathbf{PO_3H_2}$ or Ru-**COOH.**

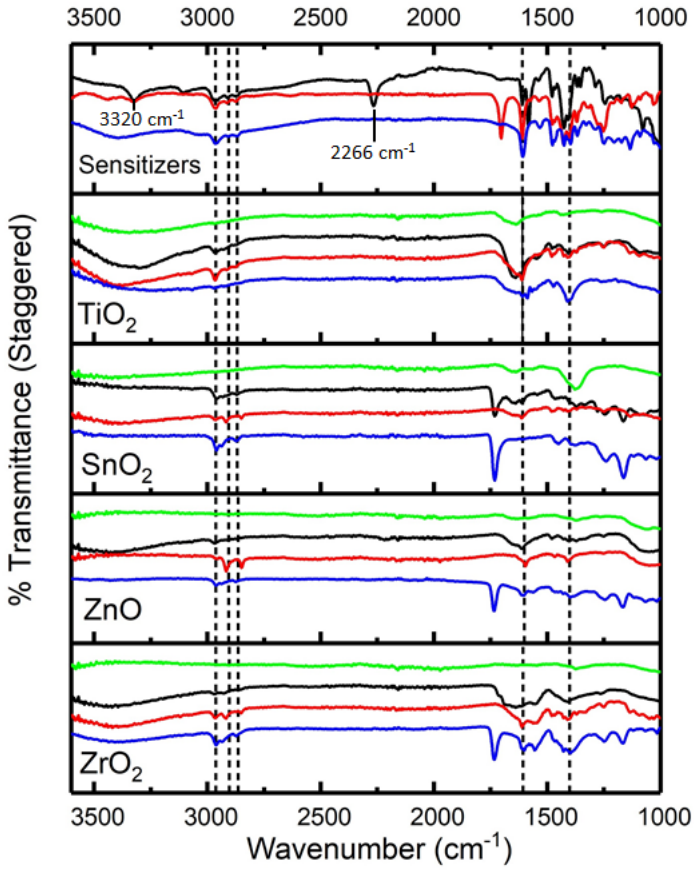

Figure 5: FTIR spectra of the ruthenium sensitizers before (top) and after functionalization on a metal oxide surface. Undyed films (green) are compared to Ru-$\mathbf{N_2}^+$ (black), Ru-$\mathbf{PO_3H_2}$ (red), and Ru-**COOH** (blue) on each examined MOx. Common peaks between the surfaces are marked by dashed lines (2960, 2910, 2870, 1610, and 1400 cm^{-1}).

The XPS spectra of Ru-$\mathbf{N_2}^+$ grafted to TiO_2 (**Figure 6**) showed the presence of a peak at 285.0 eV that has been attributed to Ru 3d as well as the absence of a diazonium peak at 403.8 eV.[28,56] Titanium peaks in the XPS spectra were standard for TiO_2, with no peak present that would be indicative of Ti(III) or a Ti-C bond (455 eV).[36,56,57] A peak at 531.6 eV representing a Ti-O-C bond was present on TiO_2 films dye-loaded with Ru-$\mathbf{N_2}^+$ that was absent on undyed TiO_2 films and TiO_2 films dye-loaded with Ru-$\mathbf{PO_3H_2}$ and Ru-**COOH**.[58–61] XPS spectra of SnO_2, ZnO, and ZrO_2 (Supplementary Information, **Figure S4**) also show no detectable change in oxidation state of the metal in the film, the presence of a Ru3d peak, and the absence of diazonium peak, indicating similar binding on all MOx.[62]

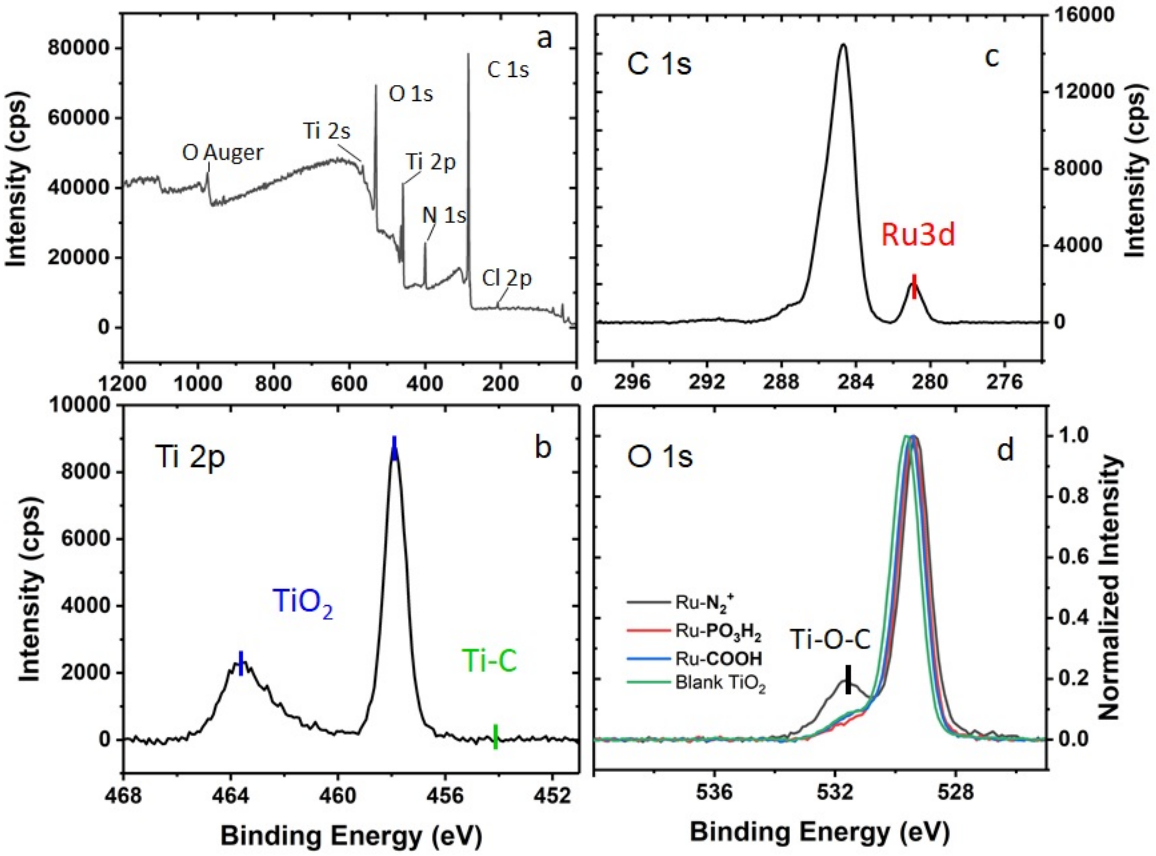

Figure 6: The XPS spectra of Ru-$\mathbf{N_2}^+$ on TiO_2. a) Spectra from 0 to 1200 eV. b) High resolution Ti 2p region with characteristic TiO_2 peaks marked in blue and absent Ti-C peak marked in green. c) High resolution C 1s region of the spectra with characteristic Ru 3d peak marked in red. d) High resolution O 1s region with overlaid spectra (intensity normalized) for Ru-$\mathbf{N_2}^+$ (black), Ru-$\mathbf{PO_3H_2}$ (red), Ru-**COOH** (blue) and blank TiO_2 (green) with characteristic peak for Ti-O-C marked in black.

The Ru(III/II) reduction potentials of both Ru-$\mathbf{PO_3H_2}$ and the electrografted Ru-$\mathbf{N_2}^+$ on MOx surfaces were measured by spectroelectrochemistry on In_2O_3:Sn at pH 1, 5, and 10 in aqueous solution and found to be $E_{1/2} = 1.07 \pm 0.02$ mV vs. NHE. Note that desorption of Ru-$\mathbf{PO_3H_2}$ was observed while performing measurements at alkaline pHs.

Surface Stability

Figure 7 shows the relative stability of Ru-$\mathbf{N_2}^+$ and Ru-$\mathbf{PO_3H_2}$ grafted on TiO_2 in aqueous solutions of pH= 7, 10, and 12. Once bound to the surface, the diazonium sensitizers were remarkably stable. Even when immersed in saturated NaOH solution for several days, diazonium-

grafted sensitizers were observed to be stable, though no formal absorption measurements were taken. In short-time-scale experiments (up to 6 hours) in the dark, Ru-$\mathbf{N_2}^+$ stability on TiO_2 was monitored up to pH 12. Ru-$\mathbf{N_2}^+$ remained stable on the surface under all examined conditions, while Ru-$\mathbf{PO_3H_2}$ at pH 7 desorbed by more than 50% in less than one minute as measured at the MLCT (**Figure 7a**). In an analogous fashion, Ru-**COOH** desorbed immediately at pHs greater than 5 (not shown). Under constant illumination (455 nm light, 100 mW/cm^2) for 24 hours at pH 12, Ru-$\mathbf{N_2}^+$ maintained >97% surface coverage as measured at the MLCT and displayed no spectral shifts (**Figure 7b**). Full spectra over 24 hours under illumination are shown in Supporting Information (**Figure S5**).

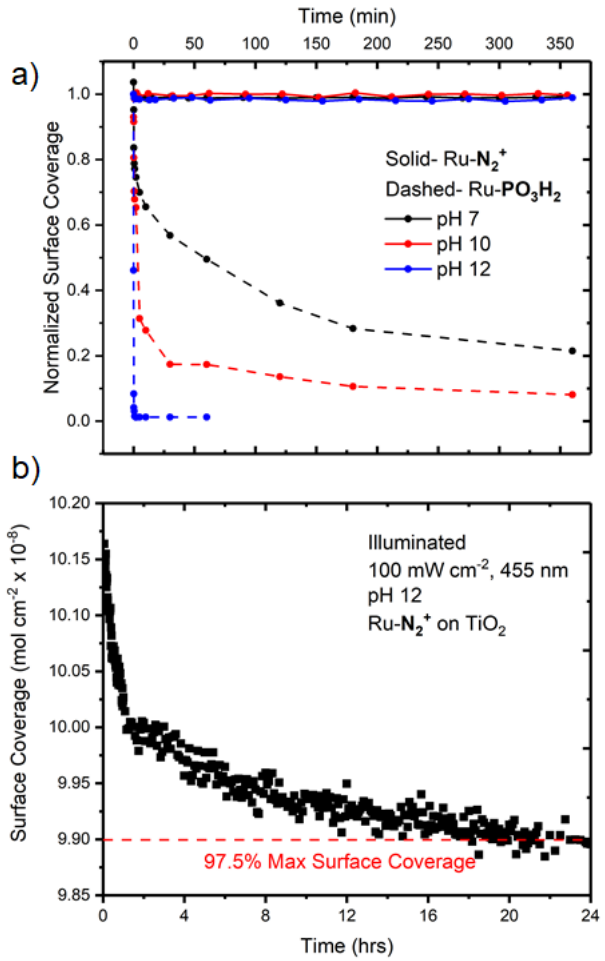

Figure 7: Surface coverage as monitored at the respective MLCTs versus time data for a) non-illuminated and b) illuminated dye-loaded TiO_2. In a) Ru-$\mathbf{N_2}^+$ (solid) was compared to Ru-$\mathbf{PO_3H_2}$ (dashed) while immersed at pH 7 (black), pH 10 (red), and pH 12 (blue) aqueous solutions over 6 hours. In b) Ru-$\mathbf{N_2}^+$ was illuminated with 455 nm, 100 mW/cm^2 light over 24 hours while immersed in pH 12 solution.

Photocurrent Measurements

Photocurrents produced by the dye-loaded MOx were measured under 1 Sun illumination with 200 mV applied potential in the presence of 50 mM electron donor (hydroquinone at pH 5 and triethanolamine at pH 12). Small photocurrents were measured on TiO_2 with either Ru-$\mathbf{N_2}^+$ or Ru-$\mathbf{PO_3H_2}$. To enhance the photocurrent amplitude, SnO_2, with a conduction band ~300 mV more positive than TiO_2, was used, and significantly larger photocurrents were attained despite lower surface coverage than on TiO_2. The dye-loaded SnO_2 photocurrents were thus considered further. Though photocurrents measured in alkaline conditions were small, at pH 12 the Ru-$\mathbf{N_2}^+$ grafted SnO_2 films produced and maintained photocurrents for >4 hours with little loss (<25%) (**Figure 8**). It should be noted that in **Figure 8**, the initial peak as the light was turned on was reproducible. It is a commonly-seen feature in dye-loaded interfaces in aqueous solution and has been attributed to electrode polarization.[63–66] UV-Visible absorption data clearly show that this initial photocurrent signature does not result from sensitizer desorption. At pH 5, photocurrents were measured for both TiO_2 and SnO_2 and both Ru-$\mathbf{N_2}^+$ and Ru-$\mathbf{PO_3H_2}$ were stable on the surface, allowing for optimal comparisons. Because surface coverage differed between these two MOx and the two sensitizers, photocurrent densities were normalized for the surface coverage. Surprisingly, Ru-$\mathbf{PO_3H_2}$ produced 7x the current of Ru-$\mathbf{N_2}^+$ on SnO_2 and almost 30x the current of Ru-$\mathbf{N_2}^+$ on TiO_2 (**Figure 8**). This stark dependence on binding group was replicable across all pH values at which Ru-$\mathbf{PO_3H_2}$ was reasonably stable on the surface for the 30 minutes that the experiment was performed (up to pH 8). Ru-**COOH** was not included for comparison because significant desorption occurred above pH 5.

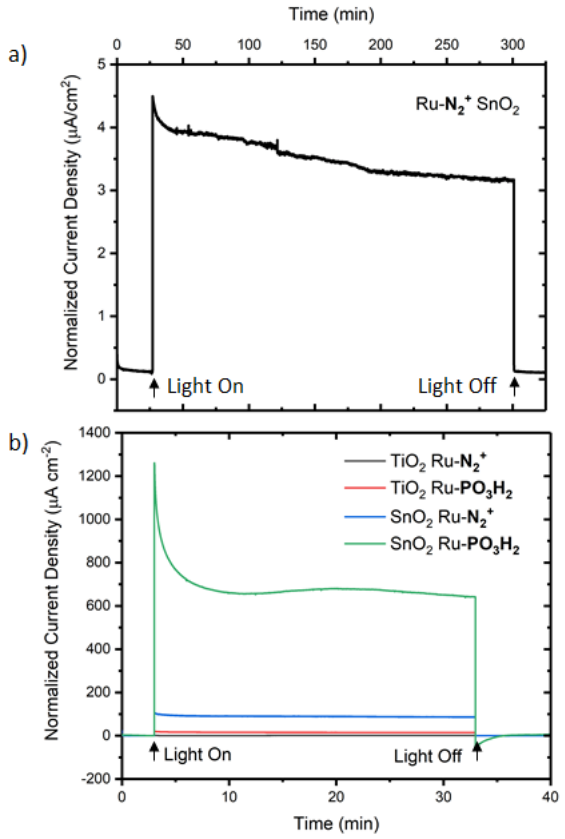

Figure 8: a) Sustained photocurrent density normalized for surface coverage measured at pH 12 for SnO_2 grafted with Ru-$\mathbf{N_2}^+$. b) Photocurrent densities normalized for surface coverage on TiO_2 with Ru-$\mathbf{N_2}^+$ (black), TiO_2 with Ru-$\mathbf{PO_3H_2}$ (red), SnO_2 with Ru-$\mathbf{N_2}^+$ (blue), and SnO_2 with Ru-$\mathbf{PO_3H_2}$ (green) were measured at pH 5. In both cases, photocurrent densities were measured under 1 Sun illumination in aqueous 0.1 M acetate buffer, 0.5 M $NaClO_4$, 50 mM sacrificial electron donor (hydroquinone at pH 5 and triethanolamine at pH 12).

Discussion

There are very few fundamental studies that report on the grafting of diazonium-based compounds to MOx colloids or thin films.[27,36–40] For example, viologen phenyl diazonium salts have recently been grafted on TiO_2 for the development of electrochromic materials.[40] These studies have shown the grafting process to be possible, but their use in solar devices is limited. [36] The functionality and stability of these grafted MOx has not been, to our knowledge, previously examined.[27,36–40] Here, the synthesis of three structurally related ruthenium sensitizers are reported that differ only by the anchoring group; Ru-$\mathbf{N_2}^+$, Ru-$\mathbf{PO_3H_2}$, and Ru-**COOH**. The electrochemical

grafting procedure reported for Ru-$\mathbf{N_2}^+$ enabled meaningful comparisons of all three sensitizers on mesoporous MOx thin films based on TiO_2, SnO_2, ZrO_2, ZnO, and In_2O_3:Sn nanoparticles. Most notably, the diazonium-loaded MOx films were stable in highly alkaline conditions, including saturated NaOH solution. Below we describe a proposed mechanism for the surface functionalization and the remarkable stability toward surface hydrolysis.

Attenuated total reflectance FTIR measurements showed that the electrografting created thin films that were not highly sensitive to the identity of the MOx or binding group: some peak shifts and differences in intensity and linewidth were observed, but most clear peaks could be found in common between all MOx and binding group varieties. The low intensity absorption bands measured on the MOx surface made further assignment ambiguous. Spectra of solid Ru-$\mathbf{N_2}^+$ exhibited intense peaks at 2266 and 3320 cm^{-1}, regions in which diazonium stretches are known to occur.[57,67] These peaks were absent when Ru-$\mathbf{N_2}^+$ was grafted to a MOx surface, indicating that the sensitizer grafted by removal of the -N_2^+ group, as seen previously in diazonium grafting of organic compounds.[26,27,36] The XPS data confirmed that grafting successfully occurred through the presence of a Ru 3d peak at 281 eV.[56] The Ti 2p peaks were in good agreement with literature values for TiO_2 (464 eV and 458 eV),[56,68] with no evidence of Ti-C bond formation that is known to give rise to a peak at 455 eV.[36] A significant band ascribed to a Ti-O-C bond was observed at 531.6 eV on films grafted with Ru-$\mathbf{N_2}^+$ that has been previously reported. [58,59,61] This band was absent in undyed TiO_2 thin films or those dye-loaded with Ru-$\mathbf{PO_3H_2}$ and Ru-**COOH**. Taken together, this data indicates that Ru-$\mathbf{N_2}^+$ formed a M-O-C bond with terminal oxygen in the lattice of TiO_2 and other MOx, as has been reported previously.[36] The covalency of this bond in comparison to films dye-loaded with Ru-$\mathbf{PO_3H_2}$ and Ru-**COOH** is likely responsible for the greater stability of grafted Ru-$\mathbf{N_2}^+$.

Azo coupling leading to the formation of multilayers has been previously reported, but evidence suggests that this did not occur here.[26,28,36] Most directly, a maximum attainable surface coverage for Ru-$\mathbf{N_2}^+$ grafted films was observed as electrografting was performed over longer times that was close to the surface coverages measured for Ru-$\mathbf{PO_3H_2}$ dye-loaded films. However, FTIR and XPS evidence was inconclusive with regard to the question of azo coupling. The FTIR spectra of all MOx surfaces grafted with Ru-$\mathbf{N_2}^+$ exhibited a peak at 1544 cm^{-1} that is in the azo (1490-1550 cm^{-1}) and C=C stretching regions.[69] In the N 1s region of XPS spectra of all Ru-$\mathbf{N_2}^+$-grafted MOx surfaces, a shoulder was present (~399 eV) that was not present for Ru-$\mathbf{PO_3H_2}$ dye-

loaded films. This may correspond to terpyridine ligands that are not complexed to Ru on the surface, as previously reported.[25,70] Taken together this evidence precludes a definitive claim of no azo coupling in Ru-$\mathbf{N_2^+}$ grafted sensitizer layers, but the observed maximum surface coverage implies that it was limited if it occurred.

Scheme 2 displays the proposed reaction mechanism between Ru-$\mathbf{N_2^+}$ and the MOx surface, which is supported by previous work.[36] Electrochemical diazonium grafting occurred when the -N_2^+ group was removed by one electron reduction (**1**) to generate an aryl radical that subsequently abstracted a hydrogen atom from the MOx surface (**2**). The newly formed surface oxygen radical is then proposed to react with a second aryl radical in solution to form a MOx-O-aryl-Ru bond (**3**). Though we propose here that two diazonium sensitizers are involved in this reaction, we cannot exclude the possibility that step **2** and **3** in **Scheme 2** might occur in a single concerted step involving a solvent molecule.

The observation of an MOx dependent "optimal potential" range for maximum surface coverage provided additional insights into the grafting mechanism. For TiO_2, SnO_2, and ZnO, Ru-$\mathbf{N_2^+}$ grafting was initiated at potentials significantly more positive than the potential at which reduction of the MOx thin films was observed by electrochemical or spectroscopic means and was absent at more negative potentials. To rationalize this "turn on" potential, it is hypothesized that a few electrons in deep trap states initiate the grafting reaction chemistry. This is consistent with the grafting being dependent on the MOx identity, as the onset potentials were correlated with the onset of MOx reduction as measured by linear voltammetry. **Scheme 2** also shows that diazonium reduction could occur at the FTO substrate, but radicals produced in this way are limited by the small surface area of FTO that is exposed. It was shown that initiation did not solely occur at the FTO, as FTO substrates that had been treated with $TiCl_4$ to block FTO exposure to the electrolyte grafted Ru-$\mathbf{N_2^+}$ equally as well as untreated slides.

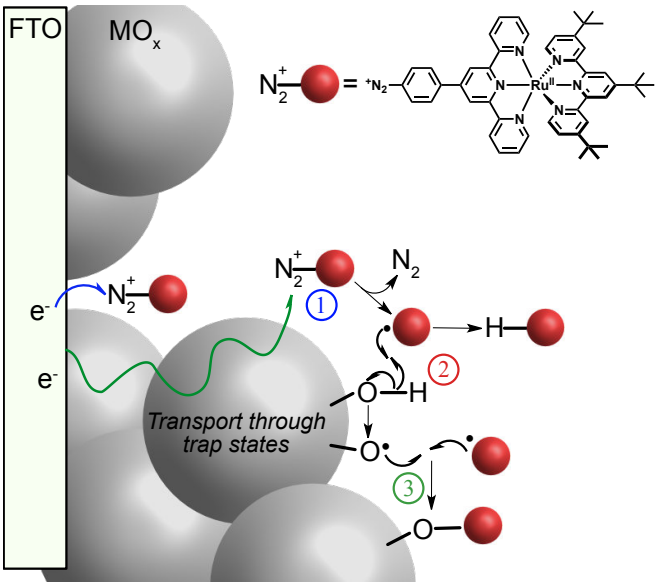

Scheme 2: Proposed electrografting mechanism for Ru-$\mathbf{N_2}^+$ with a FTO-MOx surface. The grafting occurs at the FTO (blue arrow) or by electrons in trap states (green arrow). Upon reduction of Ru-$\mathbf{N_2}^+$ (step **1**), N_2 gas is released and an aryl radical is formed that abstracts a hydrogen atom from a surface hydroxyl group yielding an unreactive ruthenium sensitizer and an M-O$^\bullet$ (step **2**). The oxygen radical then reacts with another aryl radical (formed by step (**1**)) to form the covalent M-O-C(aryl) bond (step **3**). The possibility that steps **2** and **3** occur in one concerted step cannot be ruled out nor can the possibility of CH_3CN as a H atom source.

To better understand the "turn off" potential behavior where grafting was absent at more negative potentials, undyed TiO_2 films were reduced at a potential of ~-1 V vs NHE. The black coloration of the films was maintained as the applied potential was removed and an argon purged Ru-$\mathbf{N_2}^+$ solution was introduced. No evidence for sensitizers binding to the surface was observed, indicating that electrons within the TiO_2 films did not initiate the grafting reaction chemistry and may have inhibited the reaction observed when only a few electrons were present. While speculative, it may be that the electrons present in the reduced MOx thin films rapidly react with the surface radicals generated in steps (**2**) and/or (**3**) thereby inhibiting formation of the O-C bonds. It is also possible that the increased numbers of electrons in the films at more reducing potentials increase the Ru-$\mathbf{N_2}^+$ degradation reaction rates. This possibility is supported by the spectral change in Ru-$\mathbf{N_2}^+$ solutions observed upon application of a potential more negative than the "turn off" potential. This is also consistent with the "turn off" dependence on the MOx identity, especially the much more reducing potential required to both "turn on" and "turn off" grafting in the insulating ZrO_2, as the number of electrons available for reaction with Ru-$\mathbf{N_2}^+$ should depend on

the density of states of the MOx in use. While this explanation is supported by current data, further study is underway to better understand the mechanism of grafting observed here.

The Ru-$\mathbf{N_2}^+$ grafted metal oxide thin films were remarkably stable in alkaline solution. These grafted films were observed to be stable at pH 12 for months. Films left for several days in saturated NaOH were still highly colored, yet complete desorption of Ru-$\mathbf{PO_3H_2}$ and Ru-$\mathbf{CO_2H}$ was apparent. Under 100 mW/cm^2 irradiation for 24 hours at pH 12, >97% of the initial Ru-$\mathbf{N_2}^+$ grafted TiO_2 surface coverage was maintained. Photocurrents also displayed high stability: after an initial photocurrent discharge when the light was first turned on, sustained photocurrents were measured for Ru-$\mathbf{N_2}^+$ on SnO_2 without significant change in magnitude for >4 hours at pH 12. With more acidic conditions, comparative studies with Ru-$\mathbf{PO_3H_2}$ were possible, and the photocurrent were found to be significantly larger for Ru-$\mathbf{PO_3H_2}$ than those for Ru-$\mathbf{N_2}^+$. This may arise from weaker electronic coupling to the Ti sites resulting in fewer injected electrons or from stronger electronic coupling resulting in fast back electron transfer and a net decrease in photocurrent. While such behavior is outside the scope of this study, work is underway to understand how electron injection into and back electron transfer from the MOx surface are influenced by ligand design to optimize excited state injection through this molecular linkage.

Conclusion

In conclusion, electrografting of a diazonium-substituted dye was successfully performed on a range of MOx surfaces (TiO_2, SnO_2, ZnO, ZrO_2, and In_2O_3:Sn). The observed stability in alkaline conditions represents a substantial advance from the state-of-the-art. Indeed, comparative studies with the same dye that contained -COOH and -PO_3H_2 binding groups were found to be only stable up to pH 4 and pH 7, respectively. Though recent explorations have utilized hydroxamic acid and silatrane groups with some success as binding groups in alkaline conditions, these groups are only stable to pH 11.[7] Films dye-loaded with Ru-$\mathbf{N_2}^+$ used here show remarkable stability at pH 12 and beyond. This offers immediate applications for water splitting where water oxidation catalysis is found to be most rapid in alkaline conditions. The stability that diazonium-grafted Ru-based sensitizers offer in alkali conditions allows for the pairing of sensitizers and water oxidation catalysts in conditions optimal for catalyst function. Through development of sensitizers that can be co-adsorbed or assembled with a water oxidation catalyst, this technique could be vital. In addition, the versatility of this electrografting technique to many oxide interfaces

presents an opportunity for applications to many surfaces where molecular functionality can enhance performance.

Associated Content

Supporting Information: TEM images of MOx nanoparticles, extinction coefficient of the ruthenium sensitizers, non-normalized UV-vis spectra of MOx-bound sensitizers, XPS spectra of Ru-$\mathbf{N_2}^+$ grafted on SnO_2, ZnO and ZrO_2, full spectra of Ru-$\mathbf{N_2}^+$ on TiO_2 under 24 hr illumination. This material is available free of charge on the ACS Publications website.

Author Information.

Corresponding Author

gjmeyer@email.unc.edu
ludovic@live.unc.edu

Acknowledgments.

This material is based upon work solely supported as part of the UNC EFRC: Center for Solar Fuels, an Energy Frontier Research Center funded by the U.S. Department of Energy, Office of Science, Office of Basic Energy Sciences under Award Number DE-SC0001011. L. T.-G. acknowledges personal fellowships from the Belgian American Educational Foundation (BAEF) as well as the Bourse d'Excellence Wallonie-Bruxelles (WBI.World). The authors thank the University of North Carolina Department of Chemistry Mass Spectrometry Core Laboratory and Dr. B. Ehrmann for assistance with mass spectrometry analysis. This work was performed in part at the Chapel Hill Analytical and Nanofabrication Laboratory, CHANL, a member of the North Carolina Research Triangle Nanotechnology Network, RTNN, which is supported by the National Science Foundation, Grant ECCS-1542015, as part of the National Nanotechnology Coordinated Infrastructure, NNCI.

References

(1) Desilvestro, J.; Haas, O. Metal Oxide Cathode Materials for Electrochemical Energy Storage: A Review. *J. Electrochem. Soc.* **1990**, *137*, 5C–22C.
(2) Ohta, H.; Hosono, H. Transparent Oxide Optoelectronics. *Mater. Today* **2004**, 42–51.
(3) Kolmakov, A.; Moskovits, M. Chemical Sensing and Catalysis by One-Dimensional Metal-Oxide Nanostructures. *Annu. Rev. Mater. Res.* **2004**, *34*, 151–180.
(4) Hagfeldt, A.; Boschloo, G.; Sun, L.; Kloo, L.; Pettersson, H. Dye-Sensitized Solar Cells. *Chem. Rev.* **2010**, *110*, 6595–6663.
(5) Alibabaei, L.; Luo, H.; House, R. L.; Hoertz, P. G.; Lopez, R.; Meyer, T. J. Applications of Metal Oxide Materials in Dye Sensitized Photoelectrosynthesis Cells for Making Solar Fuels: Let the Molecules Do the Work. *J. Mater. Chem. A* **2013**, *1*, 4133–4145.
(6) Brennaman, M. K.; Dillon, R. J.; Alibabaei, L.; Gish, M. K.; Dares, C. J.; Ashford, D. L.; House, R. L.; Meyer, G. J.; Papanikolas, J. M.; Meyer, T. J. Finding the Way to Solar Fuels with Dye-Sensitized Photoelectrosynthesis Cells. *J. Am. Chem. Soc.* **2016**, *138*, 13085–13102.

(7) Materna, K. L.; Crabtree, R. H.; Brudvig, G. W. Anchoring Groups for Photocatalytic Water Oxidation on Metal Oxide Surfaces. *Chem. Soc. Rev.* **2017**, *46*, 6099–6110.
(8) Brennan, B. J.; Llansola Portolés, M. J.; Liddell, P. A.; Moore, T. A.; Moore, A. L.; Gust, D. Comparison of Silatrane, Phosphonic Acid, and Carboxylic Acid Functional Groups for Attachment of Porphyrin Sensitizers to TiO_2 in Photoelectrochemical Cells. *Phys. Chem. Chem. Phys.* **2013**, *15*, 16605–16614.
(9) Zhang, L.; Cole, J. M. Anchoring Groups for Dye-Sensitized Solar Cells. *ACS Appl. Mater. Interfaces* **2015**, *7*, 3427–3455.
(10) Hanson, K.; Brennaman, M. K.; Luo, H.; Glasson, C. R. K.; Concepcion, J. J.; Song, W.; Meyer, T. J. Photostability of Phosphonate-Derivatized, Ru^{II} Polypyridyl Complexes on Metal Oxide Surfaces. *ACS Appl. Mater. Interfaces* **2012**, *4*, 1462–1469.
(11) Hyde, J. T.; Hanson, K.; Vannucci, A. K.; Lapides, A. M.; Alibabaei, L.; Norris, M. R.; Meyer, T. J.; Harrison, D. P. Electrochemical Instability of Phosphonate-Derivatized, Ruthenium(III) Polypyridyl Complexes on Metal Oxide Surfaces. *ACS Appl. Mater. Interfaces* **2015**, *7*, 9554–9562.
(12) O'Regan, B.; Grätzel, M. A Low-Cost, High-Efficiency Solar Cell Based on Dye-Sensitized Colloidal TiO_2 Films. *Nature* **1991**, *353*, 737–740.
(13) Clark, W. D. K.; Sutin, N. Spectral Sensitization of N-Type TiO_2 Electrodes by Polypyridineruthenium(II) Complexes. *J. Am. Chem. Soc.* **1977**, *99*, 4676–4682.
(14) Sprintschnik, G.; Sprintschnik, H. W.; Kirsch, P. P.; Whitten, D. G. Preparation and Photochemical Reactivity of Surfactant Ruthenium(II) Complexes in Monolayer Assemblies and at Water-Solid Interfaces. *J. Am. Chem. Soc.* **1977**, *99*, 4947–4954.
(15) Kirsch-De Mesmaeker, A.; Nasielski, J.; Willem, R. Photoelectrochemistry of $Ru(bpy)_3^{2+}$ in Basic Medium at SnO_2 and Metal Electrodes. *Bull. Soc. Chim. Belg.* **1982**, *91*, 731–742.
(16) Memming, R.; Schröppel, F. Electron Transfer Reactions of Excited Ruthenium(II) Complexes in Monolayer Assemblies at the SnO_2-Water Interface. *Chem. Phys. Lett.* **1979**, *62*, 207–210.
(17) Goodenough, J. B.; Hamnett, A.; Dare-Edwards, M. P.; Campet, G.; Wright, R. D. Inorganic Materials for Photoelectrolysis. *Surf. Sci.* **1980**, *101*, 531–540.
(18) Garcia, C. G.; Iha, M. Y. N.; Argazzi, R.; Bignozzi, C. A. 4-Phenylpyridine as Ancillary Ligand in Ruthenium(II) Polypyridyl Complexes for Sensitization of N-Type TiO_2 Electrodes. *J. Photochem. Photobiol. A Chem.* **1998**, *115*, 239–242.
(19) Hamnet, A.; Dare-Edwards, M. P.; Wright, R. D.; Seddon, K. R.; Goodenough, J. B. Photosensitization of Titanium(IV) Oxide with Tris(2,2'-bipyridine)ruthenium(II) Chloride. Surface States of Titanium(IV) Oxide. *J. Phys. Chem.* **1979**, *83*, 3280–3290.
(20) Brewster, T. P.; Konezny, S. J.; Sheehan, S. W.; Martini, L. A.; Schmuttenmaer, C. A.; Batista, V. S.; Crabtree, R. H. Hydroxamate Anchors for Improved Photoconversion in Dye-Sensitized Solar Cells. *Inorg. Chem.* **2013**, *52*, 6752–6764.
(21) Warnan, J.; Guerin, V. M.; Anne, F. B.; Pellegrin, Y.; Blart, E.; Jacquemin, D.; Pauporté, T.; Odobel, F. Ruthenium Sensitizer Functionalized by Acetylacetone Anchoring Groups for Dye-Sensitized Solar Cells. *J. Phys. Chem. C* **2013**, *117*, 8652–8660.
(22) Gou, F.; Jiang, X.; Li, B.; Jing, H.; Zhu, Z. Salicylic Acid as a Tridentate Anchoring Group for Azo -Bridged Zinc Porphyrin in Dye-Sensitized Solar Cells. *ACS Appl. Mater. Interfaces* **2013**, *5*, 12631–12637.
(23) Szpakolski, K.; Latham, K.; Rix, C.; Rani, R. A.; Kalantar-Zadeh, K. Silane: A New Linker for Chromophores in Dye-Sensitised Solar Cells. *Polyhedron* **2013**, *52*, 719–732.

(24) Takijiri, K.; Morita, K.; Nakazono, T.; Sakai, K.; Ozawa, H. Highly Stable Chemisorption of Dyes with Pyridyl Anchors over TiO_2 : Application in Dye-Sensitized Photoelectrochemical Water Reduction in Aqueous Media. *Chem. Commun.* **2017**, *53*, 3042–3045.
(25) Mahmoud, A. M.; Bergren, A. J.; McCreery, R. L. Derivatization of Optically Transparent Materials with Diazonium Reagents for Spectroscopy of Buried Interfaces. *Anal. Chem.* **2009**, *81*, 6972–6980.
(26) Pinson, J.; Podvorica, F. Attachment of Organic Layers to Conductive or Semiconductive Surfaces by Reduction of Diazonium Salts. *Chem. Soc. Rev.* **2005**, *34*, 429–439.
(27) Brymora, K.; Fouineau, J.; Eddarir, A.; Chau, F.; Yaacoub, N.; Grenèche, J. M.; Pinson, J.; Ammar, S.; Calvayrac, F. Grafting of Diazonium Salts on Oxides Surface: Formation of Aryl-O Bonds on Iron Oxide Nanoparticles. *J. Nanoparticle Res.* **2015**, *17*, 438.
(28) Troian-Gautier, L.; Martínez-Tong, D. E.; Hubert, J.; Reniers, F.; Sferrazza, M.; Mattiuzzi, A.; Lagrost, C.; Jabin, I. Controlled Modification of Polymer Surfaces through Grafting of Calix[4]arene-Tetradiazoate Salts. *J. Phys. Chem. C* **2016**, *120*, 22936–22945.
(29) Garrett, D. J.; Jenkins, P.; Polson, M. I. J.; Leech, D.; Baronian, K. H. R.; Downard, A. J. Diazonium Salt Derivatives of Osmium Bipyridine Complexes: Electrochemical Grafting and Characterisation of Modified Surfaces. *Electrochim. Acta* **2011**, *56*, 2213–2220.
(30) Troian-Gautier, L.; Valkenier, H.; Mattiuzzi, A.; Jabin, I.; Van Den Brande, N.; Van Mele, B.; Hubert, J.; Reniers, F.; Bruylants, G.; Lagrost, C.; Leroux, Y. Extremely Robust and Post-Functionalizable Gold Nanoparticles Coated with calix[4]arenes via Metal–carbon Bonds. *Chem. Commun.* **2016**, *52*, 10493–10496.
(31) Sayed, S. Y.; Bayat, A.; Kondratenko, M.; Leroux, Y.; Hapiot, P.; McCreery, R. L. Bilayer Molecular Electronics: All-Carbon Electronic Junctions Containing Molecular Bilayers Made with "Click" Chemistry. *J. Am. Chem. Soc.* **2013**, *135*, 12972–12975.
(32) Leroux, Y. R.; Hapiot, P. Nanostructured Monolayers on Carbon Substrates Prepared by Electrografting of Protected Aryldiazonium Salts. *Chem. Mater.* **2013**, *25*, 489–495.
(33) Leroux, Y. R.; Fei, H.; Noël, J. M.; Roux, C.; Hapiot, P. Efficient Covalent Modification of a Carbon Surface: Use of a Silyl Protecting Group to Form an Active Monolayer. *J. Am. Chem. Soc.* **2010**, *132*, 14039–14041.
(34) Santos, L.; Mattiuzzi, A.; Jabin, I.; Vandencasteele, N.; Reniers, F.; Reinaud, O.; Hapiot, P.; Lhenry, S.; Leroux, Y.; Lagrost, C. One-Pot Electrografting of Mixed Monolayers with Controlled Composition. *J. Phys. Chem. C* **2014**, *118*, 15919–15928.
(35) Mattiuzzi, A.; Jabin, I.; Mangeney, C.; Roux, C.; Reinaud, O.; Santos, L.; Bergamini, J.-F.; Hapiot, P.; Lagrost, C. Electrografting of calix[4]arenediazonium Salts to Form Versatile Robust Platforms for Spatially Controlled Surface Functionalization. *Nat. Commun.* **2012**, *3*, 1–8.
(36) Lund, T.; Nguyen, P. T.; Ruhland, T. Electrochemical Grafting of TiO_2-Based Photo-Anodes and Its Effect in Dye-Sensitized Solar Cells. *J. Electroanal. Chem.* **2015**, *758*, 85–92.
(37) Merson, A.; Dittrich, Th.; Zidon, Y.; Rappich, J.; Shapira, Y. Charge Transfer from TiO_2 into Adsorbed Benzene Diazonium Compounds. *Appl. Phys. Lett.* **2004**, *85*, 1075–1076.
(38) Xiong, W.; Yu, L.; Shi, H.; Phillips, D. L.; Chan, W. K. Study of Photoinduced Electron Transfer Process in Ruthenium Complex Modified Zinc Oxide Nanoparticles by Ultrafast Time-Resolved Transient Absorption Spectroscopy. *J. Inorg. Organomet. Polym. Mater.* **2017**, *27*, 39–47.

(39) Bell, K. J.; Brooksby, P. A.; Polson, M. I. J.; Downard, A. J. Evidence for Covalent Bonding of Aryl Groups to MnO_2 Nanorods from Diazonium-Based Grafting. *Chem. Commun.* **2014**, *50*, 13687–13690.
(40) Cao, L.; Fang, G.; Wang, Y. Electroreduction of Viologen Phenyl Diazonium Salts as a Strategy to Control Viologen Coverage on Electrodes. *Langmuir* **2017**, *33*, 980–987.
(41) Spampinato, V.; Tuccitto, N.; Quici, S.; Calabrese, V.; Marletta, G.; Torrisi, A.; Licciardello, A. Functionalization of Oxide Surfaces by Terpyridine Phosphonate Ligands: Surface Reactions and Anchoring Geometry. *Langmuir* **2010**, *26*, 8400–8406.
(42) Ashford, D. L.; Song, W.; Concepcion, J. J.; Glasson, C. R. K.; Brennaman, M. K.; Norris, M. R.; Fang, Z.; Templeton, J. L.; Meyer, T. J. Photoinduced Electron Transfer in a Chromophore-Catalyst Assembly Anchored to TiO_2. *J. Am. Chem. Soc.* **2012**, *134*, 19189–19198.
(43) Lainé, P.; Bedioui, F.; Ochsenbein, P.; Marvaud, V.; Bonin, M.; Amouyal, E. A New Class of Functionalized Terpyridyl Ligands as Building Blocks for Photosensitized Supramolecular Architectures. Synthesis, Structural, and Electronic Characterizations. *J. Am. Chem. Soc.* **2002**, *124*, 1364–1377.
(44) Ben Hadda, T.; Le Bozec, H. Preparation and Characterization of Ruthenium Complexes with the New 4,4′,4″-Tri-Tert-Butylterpyridine Ligand and with 4,4′-Di-Tert-Butylbipyridine. *Polyhedron* **1988**, *7*, 575–577.
(45) Preiß, J.; Jäger, M.; Rau, S.; Dietzek, B.; Popp, J.; Martínez, T.; Presselt, M. How Does Peripheral Functionalization of Ruthenium(II)-Terpyridine Complexes Affect Spatial Charge Redistribution after Photoexcitation at the Franck-Condon Point? *ChemPhysChem* **2015**, *16*, 1395–1404.
(46) Spettel, K. E.; Damrauer, N. H. Synthesis, Electrochemical Characterization, and Photophysical Studies of Structurally Tuned Aryl-Substituted Terpyridyl Ruthenium(II) Complexes. *J. Phys. Chem. A* **2014**, *118*, 10649–10662.
(47) Matheu, R.; Francàs, L.; Chernev, P.; Ertem, M. Z.; Batista, V.; Haumann, M.; Sala, X.; Llobet, A. Behavior of the Ru-Bda Water Oxidation Catalyst Covalently Anchored on Glassy Carbon Electrodes. *ACS Catal.* **2015**, *5*, 3422–3429.
(48) Heimer, T. A.; D'Arcangelis, S. T.; Farzad, F.; Stipkala, J. M.; Meyer, G. J. An Acetylacetonate-Based Semiconductor−Sensitizer Linkage. *Inorg. Chem.* **1996**, *35*, 5319–5324.
(49) Barr, T. J.; Sampaio, R. N.; DiMarco, B. N.; James, E. M.; Meyer, G. J. Phantom Electrons in Mesoporous Nanocrystalline SnO_2 Thin Films with Cation-Dependent Reduction Onsets. *Chem. Mater.* **2017**, *29*, 3919–3927.
(50) Farnum, B. H.; Morseth, Z. A.; Brennaman, M. K.; Papanikolas, J. M.; Meyer, T. J. Application of Degenerately Doped Metal Oxides in the Study of Photoinduced Interfacial Electron Transfer. *J. Phys. Chem. B* **2015**, *119*, 7698–7711.
(51) Tiwana, P.; Docampo, P.; Johnston, M. B.; Snaith, H. J.; Herz, L. M. Electron Mobility and Injection Dynamics in Mesoporous ZnO, SnO_2, and TiO_2 Films Used in Dye-Sensitized Solar Cells. *ACS Nano* **2011**, *5*, 5158–5166.
(52) DiMarco, B. N.; Motley, T. C.; Balok, R. S.; Li, G.; Siegler, M. A.; O 'Donnell, R. M.; Hu, K.; Meyer, G. J. A Distance Dependence to Lateral Self-Exchange across Nanocrystalline TiO_2. A Comparative Study of Three Homologous $Ru^{III/II}$ Polypyridyl Compounds. *J Phys Chem C* **2016**, *120*, 14226–14235.
(53) Sedghi, A.; Miankushki, H.N. Influence of $TiCl_4$ Treatment on Structure and Performance

of Dye-Sensitized Solar Cells. *Jpn. J. Appl. Phys* **2013**, *52*, 75002.
(54) Henry, J.; Livingstone, J. ITO Film Analyses by FTIR. *Infrared Phys. Technol.* **1995**, *36*, 779–784.
(55) Naghavi, N.; Marcel, C.; Dupont, L.; Rougier, A.; Leriche, J.; Guêry, C. Structural and Physical Characterisation of Transparent Conducting Pulsed Laser Deposited In_2O_3-ZnO Thin Films. *J. Mater. Chem.* **2000**, *10*, 2315–2319.
(56) Moulder, J. F.; Stickle, W. F.; Sobol, P. E.; Bomben, K. D. *Handbook of XPS*; Chastain, J., King, R. C., Eds.; Physical Electronics, Inc: Eden Prairie, Minnesota, 1992.
(57) Wagner, C. D.; Gale, L. H.; Raymond, R. H. Two-Dimensional Chemical State Plots: A Standardized Data Set for Use in Identifying Chemical States by X-Ray Photoelectron Spectroscopy. *Anal. Chem.* **1979**, *51*, 466–482.
(58) Wang, W. S.; Wang, D. H.; Qu, W. G.; Lu, L. Q.; Xu, A. W. Large Ultrathin Anatase TiO_2 Nanosheets with Exposed {001} Facets on Graphene for Enhanced Visible Light Photocatalytic Activity. *J. Phys. Chem. C* **2012**, *116*, 19893–19901.
(59) Bajestani, Z. G.; Yürüm, A.; Yürüm, Y. Significant Improvement in the Hydrogen Storage Capacity of a Reduced Graphene oxide/TiO_2 Nanocomposite by Chemical Bonding of Ti–O–C. *RSC Adv.* **2016**, *6*, 32831–32838.
(60) Zheng, T.; Feng, E.; Wang, Z.; Gong, X.; Tian, Y. Mechanism of Surface-Enhanced Raman Scattering Based on 3D Graphene–TiO_2 Nanocomposites and Application to Real-Time Monitoring of Telomerase Activity in Differentiation of Stem Cells. *ACS Appl. Mater. Interfaces* **2017**, *9*, 36596–36605.
(61) Babelon, P.; Dequiedt, A. S.; Mostéfa-Sba, H.; Bourgeois, S.; Sibillot, P.; Sacilotti, M. SEM and XPS Studies of Titanium Dioxide Thin Films Grown by MOCVD. *Thin Solid Films* **1998**, *322*, 63–67.
(62) Stranick, M. A.; Moskwa, A. SnO_2 by XPS. *Surf. Sci. Spectra* **1993**, *2*, 50–54.
(63) Alibabaei, L.; Sherman, B. D.; Norris, M. R.; Brennaman, M. K.; Meyer, T. J. Visible Photoelectrochemical Water Splitting into H_2 and O_2 in a Dye-Sensitized Photoelectrosynthesis Cell. *Proc. Nat. Acad. Sci. USA* **2015**, *112*, 5899–5902.
(64) Alibabaei, L.; Brennaman, M. K.; Norris, M. R.; Kalanyan, B.; Song, W.; Losego, M. D.; Concepcion, J. J.; Binstead, R. A.; Parsons, G. N.; Meyer, T. J. Solar Water Splitting in a Molecular Photoelectrochemical Cell. *Proc. Nat. Acad. Sci. USA* **2013**, *110*, 20008–20013.
(65) Michaux, K. E.; Gambardella, A. A.; Alibabaei, L.; Ashford, D. L.; Sherman, B. D.; Binstead, R. A.; Meyer, T. J.; Murray, R. W. Visible Photoelectrochemical Water Splitting Based on a Ru(II) Polypyridyl Chromophore and Iridium Oxide Nanoparticle Catalyst. *J. Phys. Chem. C* **2015**, *119*, 17023–17027.
(66) Sheridan, M. V.; Sherman, B. D.; Coppo, R. L.; Wang, D.; Marquard, S. L.; Wee, K.; Murakami Iha, N. Y.; Meyer, T. J. Evaluation of Chromophore and Assembly Design in Light-Driven Water Splitting with a Molecular Water Oxidation Catalyst. *ACS Energy Lett.* **2016**, *1*, 231–236.
(67) Pan, Y.; Tong, B.; Shi, J.; Zhao, W.; Shen, J.; Zhi, J.; Dong, Y. Fabrication, Characterization, and Optoelectronic Properties of Layer-by-Layer Films Based on Terpyridine-Modified MWCNTs and Ruthenium(III) Ions. *J. Phys. Chem. C* **2010**, *114*, 8040–8047.
(68) Diebold, U. The Surface Science of Titanium Dioxide. *Surf. Sci. Rep.* **2003**, *48*, 53–229.
(69) Ahmed, F.; Dewani, R.; Pervez, M. K.; Mahboob, S. J.; Soomro, S. A. Non-Destructive

FT-IR Analysis of Mono Azo Dyes. *Bulg. Chem. Commun.* **2016**, *48*, 71–77.
(70) Agnès, C.; Arnault, J.; Omnès, F.; Jousselme, B.; Billon, M.; Bidan, G.; Mailley, P. XPS Study of Ruthenium Tris-Bipyridine Electrografted from Diazonium Salt Derivative on Microcrystalline Boron Doped Diamond. *Phys. Chem. Chem. Phys.* **2009**, *11*, 11647–11654.